第 43 卷 第 13 期/2023 年 7 月/光学学报 研究论文

光学学报

氢钟测量死时间导致的光频测量统计不确定度分析

陈樱鑫[1,2,3]，卢晓同[1**]，常宏[1,2,3*]

[1]中国科学院国家授时中心时间频率基准重点实验室，陕西 西安 710600；

[2]合肥国家实验室，安徽 合肥 230088；

[3]中国科学院大学天文与空间科学学院，北京 100049

摘要 利用^{87}Sr光晶格钟与氢钟的频率比对测量了氢钟的频率稳定度。在89%的光晶格钟有效运行率下，经过约10 d的测量得出氢钟的频率稳定度，并由此推导出氢钟噪声模型的相关参数。根据氢钟噪声模型生成的随机噪声序列，对由测量死时间导致的频差进行了100次模拟，并以模拟结果的1倍标准差为测量不确定度。不同有效运行率下，氢钟测量不确定度的计算结果表明，由氢钟测量死时间导致的不确定度随有效运行率的增加而减小，且在有效运行率小于10%时，增加总的测量时间可以显著减小测量不确定。

关键词 测量；光频测量；氢钟噪声模型；光晶格钟；稳定度

中图分类号 O562.5 **文献标志码** A **DOI**：10.3788/AOS230444

1 引 言

光钟技术在近20年里发展迅速，已经实现了9.4×10^{-19}的系统不确定度和4.8×10^{-17}@1 s量级的频率稳定度[1-2]，已在验证广义相对论[3-4]、测量精细结构常数随时间可能产生的微变[5-6]、探测超轻玻色暗物质[7]、量子模拟[8-10]和相对论测地学等领域得到重要应用[11]。随着越来越多的光钟系统不确定度进入10^{-18}量级[1,12-18]，以及光钟绝对频率测量精度从根本上受限于^{133}Cs喷泉钟的系统不确定度[19-20]，利用光频跃迁重新定义时间的基本单位（秒）已被提议[21]。第27次国际计量大会（CGPM）正式通过决议：将在2026年举办的第28次CGPM上讨论选择重定义秒的光频标类型；在2030年举办的第29次CGPM上正式利用光频跃迁定义秒[22]。

在2018年国际计量委员会（CIPM）就利用光钟作为“秒”定义的装置提出的5个具有里程碑意义的建议[21]中就包括“光钟绝对频率的测量不确定度小于3×10^{-16}”。尽管通过与绝对频率已知的光钟和作为主频标或二级频标的喷泉钟进行频率比对能够确定待测光钟的绝对频率[23-24]，但是由于很多单位没有^{133}Cs喷泉钟或者其他频率已知的喷泉钟或光钟，目前光钟绝对频率测量的最主要方式为通过卫星链路溯源国际原子时（TAI）。该技术需要利用氢钟作为本地振荡器并依次溯源本地协调世界时、协调世界时、TAI和由主频标钟组定义的秒。在这个复杂的溯源过程中，氢钟测量死时间（由于光钟不连续运行）导致的统计不确定度是光钟绝对频率测量不确定度的最主要来源之一[25-28]。在扣除氢钟频率漂移（本实验氢钟的相对频率漂移速率为-6.4×10^{-17} d^{-1}）的贡献后，氢钟测量死时间导致的统计不确定度可通过数值模拟获得。该方法需要知道氢钟噪声模型的准确参数，包括相位白噪声、频率白噪声、频率闪烁噪声和随机游走噪声[25-28]。氢钟噪声模型可以通过多台氢钟相互比对或者氢钟与稳定度很高的光钟进行频率比对来获得[25-28]。

本文将光学频率梳对^{87}Sr光晶格钟（OLC）与氢钟进行频率比对。通过计算频率比对稳定度并结合氢钟噪声模型进行拟合，获得氢钟噪声模型的相关参数；根据氢钟噪声模型，利用商用软件Stable32分别产生86400×5 s、86400×10 s和86400×30 s三种测量时长的随机噪声序列，并分别计算三种测量时长下氢钟测量死时间（有效运行率）对光频测量统计不确定度的影响。

2 实验装置

光晶格钟与氢钟频率比对的实验装置如图1所

收稿日期：2023-01-05；**修回日期**：2023-02-08；**录用日期**：2023-03-06；**网络首发日期**：2023-03-13

基金项目：国家自然科学基金（12203057）、中国科学院战略性先导科技专项（B类）（XDB35010202）

通信作者：*changhong@ntsc.ac.cn；** luxiaotong@ntsc.ac.cn

示，其中DDS为直接数字频率合成器，ULE为超低膨胀玻璃，AOM_1和AOM_2为声光调制器，f_b为^{87}Sr光晶格钟输出的光信号与光学频率梳的拍频，f_{ceo}为光学频率梳的载波包络相位，f_r为光学频率梳的重复频率，伺服系统$servo_1$和$servo_2$分别用于锁定f_{ceo}和f_r。从温度为500 ℃的锶炉喷出的气态^{87}Sr原子依次经过内径为0.8 mm的不锈钢毛细管和由461 nm激光（相对于$|^1S_0, F=9/2\rangle \rightarrow |^1P_1, F=11/2\rangle$跃迁频率负失谐15 MHz）组成的二维光学准直系统来减小原子的发散角。然后，原子经过减速光和多匝线圈塞曼减速器后动能降低（增加速度低于50 m/s的原子数量），并到达由磁场和俘获光场形成的磁光阱（MOT）区域。经蓝MOT（俘获光波长为461 nm，相对于$|^1S_0, F=9/2\rangle \rightarrow |^1P_1, F=11/2\rangle$跃迁频率负失谐35 MHz）和红MOT（俘获光波长为689 nm，相对于$|^1S_0, F=9/2\rangle \rightarrow |^3P_1, F=11/2\rangle$跃迁频率负失谐约500 kHz）俘获和减速后，原子的温度被降低至3 μK左右，数量在10^6量级。在红MOT阶段，需要利用689 nm匀化光（其相对于$|^1S_0, F=9/2\rangle \rightarrow |^3P_1, F=9/2\rangle$跃迁负失谐约150 kHz）使原子在10个塞曼子能级间快速重新分布，以增加原子数量并提高冷却效率[29]。红MOT俘获结束后，俘获光和磁场迅速被关断，原子被装载进沿水平方向的一维光晶格。晶格光的波长约为813.42 nm，偏振方向沿重力方向，其频率被锁定在一个10 cm长的ULE超稳腔上。待未被晶格俘获的原子离开探测区域后，利用3组亥姆霍兹线圈来消除水平方向的杂散磁场，在竖直（重力）方向保持约50 mG（1 T=10^4 G）的磁场来定义量子化轴。一束沿重力方向的689 nm极化光（相对于$|^1S_0, F=9/2\rangle \rightarrow |^3P_1, F=9/2\rangle$跃迁频率负失谐约50 kHz）单次穿过晶格。极化光的偏振为左（右）旋圆偏振，可将原子自旋极化到$m_F=-9/2$（$m_F=+9/2$）的塞曼子能级上。光晶格的初始阱深为$110E_R$（E_R为晶格光子反冲能量），自旋极化完成后，阱深在15 ms内被绝热地减小至$45E_R$，保持该阱深15 ms以使动能较高的原子逃离晶格，然后在15 ms内绝热地将阱深增加至$110E_R$。经过上述“能量过滤”[30]过程后，原子的轴向和径向温度分别被降低至1.2 μK和2.3 μK，原子数量约为10^3。

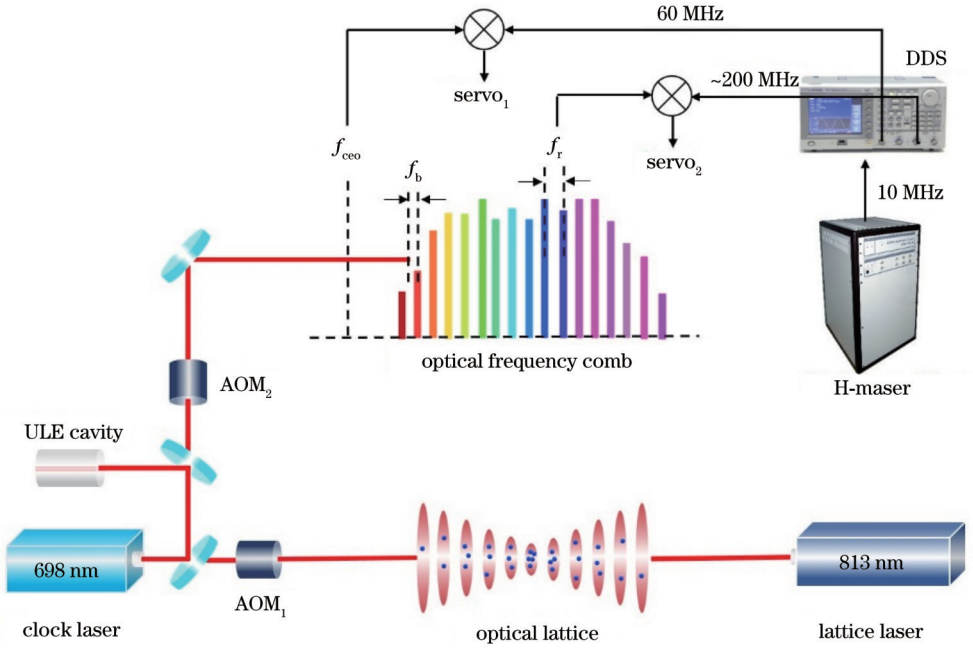

图1　光晶格钟与氢钟频率比对实验装置

Fig. 1　Experimental setup of frequency comparison between optical lattice clock and hydrogen maser

在完成态制备后，利用与晶格光完全重合的钟激光与原子相互作用来获得钟激光与^{87}Sr钟跃迁（$|^1S_0, F=9/2\rangle \rightarrow |^3P_0, F=9/2\rangle$）频率的差异。为了减小钟激光的噪声，钟激光的相位被锁定在一个长20 cm的ULE超稳腔上。对电光调制晶体温度和进腔光功率进行主动稳定后，钟激光的稳定度为4×10^{-16}[31]。钟激光与晶格光的偏振一致，从晶格反射镜方向入射且有50%的钟激光被反射镜反射，用于将钟激光的相位参考至晶格反射镜上，以消除一阶多普勒效应[32]。由于光晶格钟的稳定度比氢钟高2个数量级以上，光晶格钟与氢钟的频率比对稳定度表征了氢钟的稳定度。光学频率梳（OFC，IMRA）的重复频率（$f_r\approx200$ MHz）和载波包络相位（$f_{ceo}=60$ MHz）与DDS（Tektronix，AFG3252C）输出的频率混频滤波后，通过反馈OFC压电陶瓷、电光调制晶体锁定重复频率，通过反馈泵浦光功率和电光调制晶体锁定载波包络相位。DDS的频率外参考至氢钟（VCH-1003M，

No. 5085)输出的 10 MHz 信号上，因此通过频率计数器(KEYSIGHT 53230A)记录 OFC 与光晶格钟输出光信号的拍频(f_b)就能够获得氢钟的频率抖动，进而获得氢钟的频率稳定度。

3 实验结果与分析

为了消除一阶塞曼频移，钟激光的频率通过“四点锁定”方案锁定至 $|^1S_0, m_F=+9/2\rangle \rightarrow |^3P_0, m_F=+9/2\rangle$ 和 $|^1S_0, m_F=-9/2\rangle \rightarrow |^3P_0, m_F=-9/2\rangle$ 跃迁频率的平均值处[33]，通过 AOM_2 将到达 OFC 的钟激光频率调节至两个跃迁的平均值处(本实验中，每 4 s 反馈一次)。为了避免环境温度、原子数和磁场强度等参数变化对测量结果的影响，在设定 AOM_2 调制信号频率时，已经事先根据系统评估结果(系统频移修正量总的不确定度最大值为 5.1×10^{-17})扣除了各项系统频移[31]，即到达 OFC 的钟激光频率对应无外场扰动的 ^{87}Sr 钟跃迁频率。为了更好地提取氢钟的噪声，将 ^{87}Sr 光晶格钟闭环运行了约 10 d，频率计数器(参考至氢钟)记录的 f_b 如图 2(a)所示。测量过程中，直流斯塔克频移、钟激光和晶格光交流斯塔克频移、背景气体碰撞频移的系统频移修正量保持不变，黑体辐射频移、二阶塞曼频移、密度频移和伺服误差则根据监测的相关系统参数(温度平均值及相应的不确定度、磁场大小、原子散射的荧光信号强度和伺服信号)进行实时修正。光晶格钟的有效运行率约为 89%，计算图 2(a)所示的 f_b 相对于 ^{87}Sr 钟跃迁频率的交叠艾伦偏差，结果如图 2(b)所示。可以看到，氢钟与本地协调世界时比对的短期稳定度较差，表明协调世界时的噪声大于氢钟，因此在光钟溯源国际原子时的过程中需要用噪声小且能连续运行的氢钟作为媒介，以减小光钟不连续运行带来的统计误差[34]。根据随机噪声模型，假定氢钟噪声主要包括相位白噪声(A_1)、频率白噪声(A_2)、频率闪烁噪声(A_3)和随机游走噪声(A_4)。考虑到各类噪声相互独立，可根据各类噪声艾伦偏差随时间的变化趋势来构建拟合函数 $y(\tau)=\sqrt{A_1^2\tau^{-2}+A_2^2\tau^{-1}+A_3^2\tau^0+A_4^2\tau^1}$($\tau$ 为测量时间)，表征氢钟稳定度。通过该函数拟合光钟与氢钟的频率比对稳定度，可得到 4 个待测参数 $A_1=2.21\times10^{-13}\,(\tau/\mathrm{s})^{-1}$、$A_2=3.05\times10^{-13}\,(\tau/\mathrm{s})^{-0.5}$、$A_3=6.01\times10^{-16}$ 和 $A_4=4.49\times10^{-19}\,(\tau/\mathrm{s})^{0.5}$。

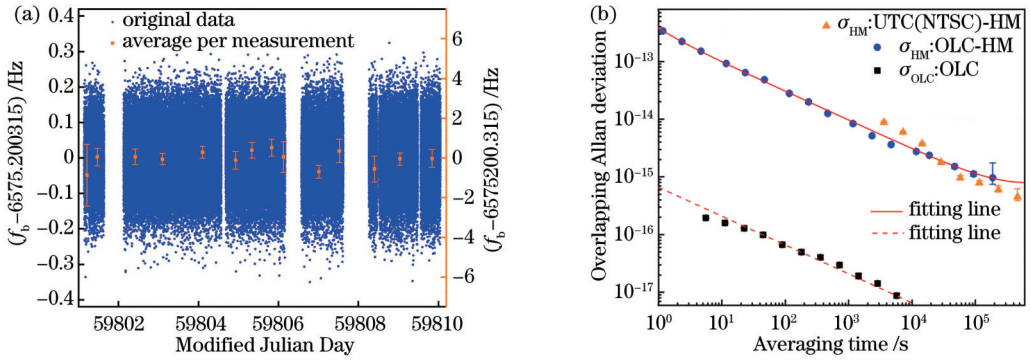

图 2 氢钟稳定度测量。(a)^{87}Sr 光晶格钟与光学频率梳拍频信号 f_b，其中方点表示每次测量的均值，误差棒为 1σ 标准差；(b)f_b 相对于 ^{87}Sr 钟跃迁频率的交叠艾伦偏差，其中圆点表示氢钟与光晶格钟频率比对的稳定度，实线表示随机噪声模型拟合的结果，方点表示光晶格钟的自比对稳定度，虚线表示线性拟合结果[固定斜率为 −0.5，自比对稳定度为 $6.6\times10^{-16}\,(\tau/\mathrm{s})^{-0.5}$]，三角点为氢钟与本地协调世界时比对的稳定度

Fig. 2 Stability measurement of the H-maser. (a) Beat frequency f_b between ^{87}Sr optical lattice clock and optical frequency comb (the squares represent the mean value of each measurement and error bars indicate 1σ standard deviation); (b) overlapping Allan deviation between f_b and the frequency of ^{87}Sr optical lattice clock {circles indicate the stability calculated from the comparison data between the OLC and H-maser, the solid curve is the fitting result using the stochastic noise model, squares are the interleaved self-comparison stability of the OLC, the dotted line is the linear fitting [with a fixed slope of −0.5, showing an interleaved self-comparison stability of $6.6\times10^{-16}\,(\tau/\mathrm{s})^{-0.5}$], and the triangles are the stability of the hydrogen clock by comparing with the local Coordinated Universal Time (UTC-NTSC)}

尽管在光钟绝对频率测量过程中氢钟往往能保持连续运行，但光钟运行中断会导致氢钟与光钟的比对不连续。在最后数据处理的过程中，只能用连续运行的氢钟频率来推断光钟的绝对频率。然而，氢钟的随机噪声可能导致部分测量与整体数据间噪声均值不一致，最终影响光钟绝对频率的测量结果。为了推断由氢钟测量死时间导致的测量不确定度，需要根据氢钟噪声模型产生随机噪声序列，且其时长与总的测量时间相同，并计算有效测量时间内的数据与整体数据的差异[26,35]。根据单次模拟得到的结果只能得到一个可能的值，因此需要重复模拟多次并以这些结果的 1 倍标准差作为氢钟测量死时间导致的测量不确定度。根据氢钟噪声模型，用商用软件 Stable32 分别产生 86400×5 s、86400×10 s 和 86400×30 s 三种测量时长

的随机噪声[图 3(a)],分别对应 5 d、10 d 和 30 d 的总测量时长。图 3(b)所示为根据图 3(a)的数据计算得到的稳定度,它们均与拟合得到的氢钟噪声模型相符,表明 Stable32 产生的随机噪声序列可以很好地表征氢钟的实际噪声。对每种情况分别模拟 100 次,分别计算不同氢钟有效运行率下有效数据与整体数据的频差,并将这 100 次模拟结果的 1 倍标准差作为最终的不确定度。图 4 展示了氢钟运行率(有效测量时长与总测量时长的比值)与光钟绝对频率测量统计不确定度的关系,可以看到,由氢钟测量死时间导致的测量不确定度随着氢钟有效运行率的增加而减小。整体而言,总测量时间为 5 d 的测量不确定度要高于总测量时间为 10 d 和 30 d 的情况。当氢钟(或者光钟)有效运行率小于 10% 时,通过增加总的测量时长可以显著减小统计不确定度;当运行率高于 10% 时,增加总的测量时长无法有效降低测量不确定度(尽管高于 90% 时,3 组数据的差异看似很大,但由于是对数坐标,3 组数据间的差异在 10^{-17} 量级)。

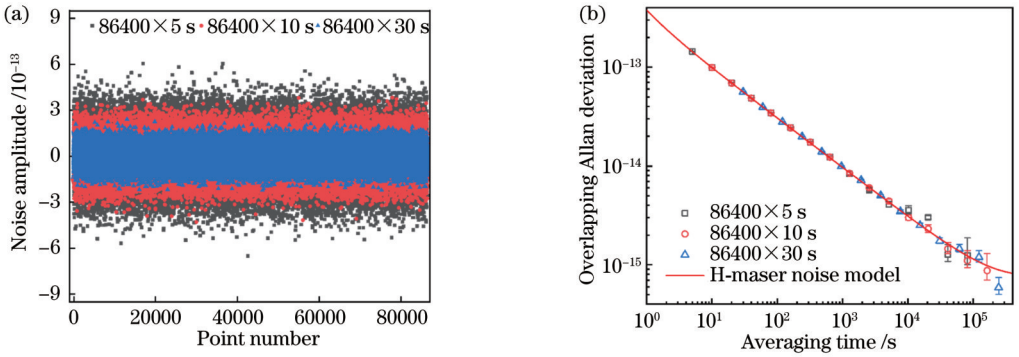

图 3　氢钟随机噪声模拟。(a)根据氢钟噪声模型分别产生 86400×5 s、86400×10 s 和 86400×30 s 三种随机噪声序列;(b)根据所产生的噪声序列计算其对应的交叠 Allan 偏差,其中实线为图 2(b)给出的氢钟噪声模型

Fig. 3　Simulations of H-maser random noise. (a) Three types of random noise sequences of 86400×5 s, 86400×10 s, and 86400×30 s generated by H-maser noise model; (b) calculated overlapping Allan deviation according to three types of noise sequences, and solid line indicates the H-maser noise model obtained from Fig. 2(b)

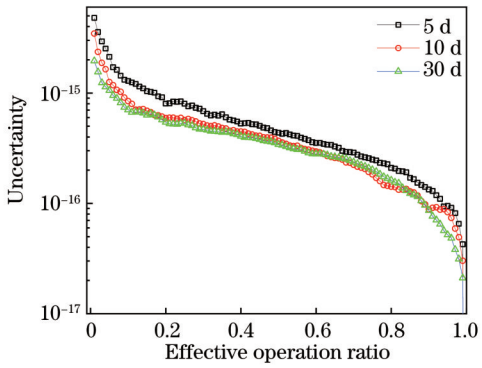

图 4　不同有效运行率下的氢钟测量不确定度

Fig. 4　H-maser measurement uncertainty as a function of the effective operation ratio

4　结　　论

利用 ^{87}Sr 光晶格钟与氢钟长时间的频率比对,测量了氢钟的频率稳定度,并通过拟合氢钟频率稳定度数据获得了氢钟噪声模型参数——相位白噪声为 $2.21\times10^{-13}(\tau/\mathrm{s})^{-1}$,频率白噪声为 $3.05\times10^{-13}(\tau/\mathrm{s})^{-0.5}$,频率闪烁噪声为 6.01×10^{-16},随机游走噪声为 $4.49\times10^{-19}(\tau/\mathrm{s})^{0.5}$。利用 Stable32 软件根据噪声模型产生随机噪声序列的方式评估了光钟绝对频率测量不确定度与氢钟有效运行率的关系,计算结果表明,由氢钟测量死时间导致的测量不确定度随有效运行率的增加而减小,且在有效运行率小于 10% 时,增加总的测量时间可显著减小不确定度。所提方法可广泛应用于通过溯源 TAI 的方式测量光钟绝对频率,且为选择光钟有效运行率以减小由氢钟测量死时间导致的测量不确定度提供重要参考。

参　考　文　献

[1] Brewer S M, Chen J S, Hankin A M, et al. $^{27}Al^{+}$ quantum-logic clock with a systematic uncertainty below 10^{-18}[J]. Physical Review Letters, 2019, 123(3): 033201.

[2] Oelker E, Hutson R B, Kennedy C J, et al. Demonstration of 4.8×10^{-17} stability at 1 s for two independent optical clocks[J]. Nature Photonics, 2019, 13(10): 714-719.

[3] Sanner C, Huntemann N, Lange R, et al. Optical clock comparison for Lorentz symmetry testing[J]. Nature, 2019, 567(7747): 204-208.

[4] Bothwell T, Kennedy C J, Aeppli A, et al. Resolving the gravitational redshift across a millimetre-scale atomic sample[J]. Nature, 2022, 602(7897): 420-424.

[5] Godun R M, Nisbet-Jones P B R, Jones J M, et al. Frequency ratio of two optical clock transitions in $^{171}Yb^{+}$ and constraints on the time variation of fundamental constants[J]. Physical Review Letters, 2014, 113(21): 210801.

[6] Huntemann N, Lipphardt B, Tamm C, et al. Improved limit on a temporal variation of mp/me from comparisons of Yb^{+} and Cs atomic clocks[J]. Physical Review Letters, 2014, 113(21): 210802.

[7] Beloy K, Bodine M I, Bothwell T, et al. Frequency ratio measurements at 18-digit accuracy using an optical clock network

[J]. Nature, 2021, 591(7851): 564-569.
[8] Yin M J, Wang T, Lu X T, et al. Rabi spectroscopy and sensitivity of a floquet engineered optical lattice clock[J]. Chinese Physics Letters, 2021, 38(7): 073201.
[9] Lu X T, Wang T, Li T, et al. Doubly modulated optical lattice clock: interference and topology[J]. Physical Review Letters, 2021, 127(3): 033601.
[10] Yin M J, Lu X T, Li T, et al. Floquet engineering Hz-level Rabi spectra in shallow optical lattice clock[J]. Physical Review Letters, 2022, 128(7): 073603.
[11] Grotti J, Koller S, Vogt S, et al. Geodesy and metrology with a transportable optical clock[J]. Nature Physics, 2018, 14(5): 437-441.
[12] Bloom B J, Nicholson T L, Williams J R, et al. An optical lattice clock with accuracy and stability at the 10^{-18} level[J]. Nature, 2014, 506(7486): 71-75.
[13] Nicholson T L, Campbell S L, Hutson R B, et al. Systematic evaluation of an atomic clock at 2×10^{-18} total uncertainty[J]. Nature Communications, 2015, 6(1): 1-8.
[14] Bothwell T, Kedar D, Oelker E, et al. JILA SrI optical lattice clock with uncertainty of 2.0×10^{-18}[J]. Metrologia, 2019, 56(6): 065004.
[15] McGrew W F, Zhang X, Fasano R J, et al. Atomic clock performance enabling geodesy below the centimetre level[J]. Nature, 2018, 564(7734): 87-90.
[16] Ushijima I, Takamoto M, Das M, et al. Cryogenic optical lattice clocks[J]. Nature Photonics, 2015, 9(3): 185-189.
[17] Huntemann N, Sanner C, Lipphardt B, et al. Single-ion atomic clock with 3×10^{-18} systematic uncertainty[J]. Physical Review Letters, 2016, 116(6): 063001.
[18] Lu B K, Sun Z, Yang T, et al. Improved evaluation of BBR and collisional frequency shifts of NIM-Sr2 with 7.2×10^{-18} total uncertainty[J]. Chinese Physics Letters, 2022, 39(8): 080601.
[19] Le Targat R, Lorini L, Le Coq Y, et al. Experimental realization of an optical second with strontium lattice clocks[J]. Nature Communications, 2013, 4(1): 1-9.
[20] Schwarz R, Dörscher S, Al-Masoudi A, et al. Long term measurement of the ^{87}Sr clock frequency at the limit of primary Cs clocks[J]. Physical Review Research, 2020, 2(3): 033242.
[21] Riehle F, Gill P, Arias F, et al. The CIPM list of recommended frequency standard values: guidelines and procedures[J]. Metrologia, 2018, 55(2): 188-200.
[22] CGPM. 27th CGPM: key outcomes and documents[EB/OL]. [2022-11-08]. https://www.bipm.org/en/cgpm-2022/documents.
[23] Matsubara K, Hachisu H, Li Y, et al. Direct comparison of a Ca^{+} single-ion clock against a Sr lattice clock to verify the absolute frequency measurement[J]. Optics Express, 2012, 20(20): 22034-22041.
[24] Yamaguchi A, Fujieda M, Kumagai M, et al. Direct comparison of distant optical lattice clocks at the 10^{-16} uncertainty[J]. Applied Physics Express, 2011, 4(8): 082203.
[25] Lin Y G, Wang Q, Meng F, et al. A ^{87}Sr optical lattice clock with 2.9×10^{-17} uncertainty and its absolute frequency measurement[J]. Metrologia, 2021, 58(3): 035010.
[26] Hobson R, Bowden W, Vianello A, et al. A strontium optical lattice clock with 1×10^{-17} uncertainty and measurement of its absolute frequency[J]. Metrologia, 2020, 57(6): 065026.
[27] Kim H, Heo M S, Park C Y, et al. Absolute frequency measurement of the ^{171}Yb optical lattice clock at KRISS using TAI for over a year[J]. Metrologia, 2021, 58(5): 055007.
[28] Luo L M, Qiao H, Ai D, et al. Absolute frequency measurement of an Yb optical clock at the 10^{-16} level using International Atomic Time[J]. Metrologia, 2020, 57(6): 065017.
[29] Mukaiyama T, Katori H, Ido T, et al. Recoil-limited laser cooling of ^{87}Sr atoms near the Fermi temperature[J]. Physical Review Letters, 2003, 90(11): 113002.
[30] Falke S, Lemke N, Grebing C, et al. A strontium lattice clock with 3×10^{-17} inaccuracy and its frequency[J]. New Journal of Physics, 2014, 16(7): 073023.
[31] Lu X T, Guo F, Wang Y B, et al. Absolute frequency measurement of the ^{87}Sr optical lattice clock at NTSC using international atomic time[J]. Metrologia, 2023, 60(1): 015008.
[32] Falke S, Misera M, Sterr U, et al. Delivering pulsed and phase stable light to atoms of an optical clock[J]. Applied Physics B, 2012, 107(2): 301-311.
[33] 林弋戈, 方占军. 锶原子光晶格钟[J]. 物理学报, 2018, 67(16): 160604.
Lin Y G, Fang Z J. Strontium optical lattice clock[J]. Acta Physica Sinica, 2018, 67(16): 160604.
[34] Hachisu H, Fujieda M, Kumagai M, et al. Absolute frequency measurement at 10^{-16} level based on the international atomic time[J]. Journal of Physics: Conference Series, 2016, 723: 012042.
[35] Hachisu H, Petit G, Nakagawa F, et al. SI-traceable measurement of an optical frequency at the low 10^{-16} level without a local primary standard[J]. Optics Express, 2017, 25(8): 8511-8523.

Analysis of Statistical Uncertainty of Optical Frequency Measurement Due to Measurement Dead Time of Hydrogen Maser

Chen Yingxin[1,2,3], Lu Xiaotong[1**], Chang Hong[1,2,3*]

[1]*Key Laboratory of Time and Frequency Primary Standards, National Time Service Center, Chinese Academy of Sciences, Xi'an* 710600, *Shaanxi, China*;

[2]*Hefei National Laboratory, Hefei* 230088, *Anhui, China*;

[3]*School of Astronomy and Space Science, University of Chinese Academy of Sciences, Beijing* 100049, *China*

Abstract

Objective Optical clocks have developed rapidly in the past 20 years and have achieved a systematic uncertainty of 9.4×10^{-19} and frequency stability of 4.8×10^{-17}@1 s. Except for the generation of standard time and frequency, optical clocks have many important applications, such as verification of general relativity, measurement of possible variation of the fine

structure constant with time, detection of ultralight bosonic dark matter, quantum simulation, and relativistic geodesy. As more and more systematic uncertainty of the optical clock enters the order of 10^{-18}, and the absolute frequency measurement accuracy of the optical clock is fundamentally limited by the systematic uncertainty of the ^{133}Cs fountain clock, it has been proposed to use optical frequency transition to redefine the second in the international system of units. The 27th General Conference of Weights and Measures (CGPM) officially passed a resolution: The 28th CGPM will be held in 2026 to discuss the choice of optical clock types for redefining the second, and the optical frequency transition will be formally used to define the second expected in 2030. One of the main methods of absolute frequency measurement of optical clocks is to trace the international atomic time through a satellite link, and measurement uncertainty of less than 3×10^{-16} is a precondition for the redefinition of the second in the international system of units by the optical frequency transition. In this complex tracing link, the uncertainty caused by the measurement dead time of the hydrogen maser is one of the main sources of absolute frequency measurement uncertainty for most optical clocks. After removing the contribution of frequency drift of the hydrogen maser, the statistical uncertainty caused by the measurement dead time of the hydrogen maser can be obtained by numerical simulation. This method needs to know the relevant parameters of the noise model of the hydrogen maser accurately and then generate the relevant random noise sequences by software.

Methods In this paper, the frequency comparison between the ^{87}Sr optical lattice clock and hydrogen maser is made by using an optical frequency comb. By calculating the stability of the frequency ratio and fitting with the function of $y(\tau)=\sqrt{A_1^2\tau^{-2}+A_2^2\tau^{-1}+A_3^2\tau^0+A_4^2\tau^1}$ (τ is the measurement time, and A_{1-4} indicate the amplitudes of phase white noise, frequency white noise, frequency flicker noise, and random walk noise, respectively), the values of A_{1-4} are obtained. Finally, according to the noise model of the hydrogen maser, we use the software to generate random noise series of 86400×5 s, 86400×10 s, and 86400×30 s, respectively, and calculate the statistical uncertainty of optical frequency measurement under different effective operating rates (the measurement dead time of the hydrogen maser) and total measurement durations.

Results and Discussions The parameters of the noise model of the hydrogen maser are determined as $A_1=2.21\times10^{-13}\,(\tau/\mathrm{s})^{-1}$, $A_2=3.05\times10^{-13}\,(\tau/\mathrm{s})^{-0.5}$, $A_3=6.01\times10^{-16}$, and $A_4=4.49\times10^{-19}\,(\tau/\mathrm{s})^{0.5}$, respectively after about 10-day measurement with an effective operating rate of 89% [Fig. 2(b)]. The frequency difference caused by the measurement dead time of the hydrogen maser is simulated 100 times by using the method of generating random noise sequences (using the software of Stable32) according to the noise model. Three types of random noise sequences are generated with a total measurement time of 86400×5 s, 86400×10 s, and 86400×30 s, respectively. The difference in the mean frequency from the total mean over partial times is calculated for the specific case. Each case is repeated by 100 times, and the measurement uncertainty caused by the measurement dead time of the hydrogen maser is represented by the 1 times standard deviation of these results. Figure 4 shows the calculation results of the measurement uncertainty as a function of the effective operating rate. The measurement uncertainty due to the measurement dead time decreases with the increase in the effective operating rate, and when the effective operating rate is less than 10% or so, increasing the total measurement time can significantly reduce the measurement uncertainty.

Conclusions In this study, the frequency stability of the hydrogen maser is measured by comparing the ^{87}Sr optical lattice clock (with an 89% effective operating ratio and a total measurement time of about 10 days) with the hydrogen maser for a long time. By fitting the data of the frequency stability of the hydrogen maser with the noise model function, the influence of each noise of the hydrogen maser is determined as $2.21\times10^{-13}\,(\tau/\mathrm{s})^{-1}$ for phase white noise, $3.05\times10^{-13}\,(\tau/\mathrm{s})^{-0.5}$ for frequency white noise, 6.01×10^{-16} for frequency flicker noise, and $4.49\times10^{-19}\,(\tau/\mathrm{s})^{0.5}$ for random walk noise. The calculation results indicate that the measurement uncertainty caused by the measurement dead time of the hydrogen maser decreases with the increase in the effective operating rate, and when the effective operating rate is less than 10% or so, increasing the total measurement time can significantly reduce the uncertainty. This work can be widely used to measure the absolute frequency of optical clocks by tracing the international atomic time and provide an important reference for selecting the effective operating rate of the optical clock to reduce the measurement uncertainty caused by the measurement dead time of the hydrogen maser.

Key words measurement; optical frequency measurement; noise model of hydrogen maser; optical lattice clock; stability